Magnetic moments of low-lying states in tin isotopes within the nucleon-pair approximation

H. Jiang,[1,2,3,*] Y. Lei,[4] C. Qi ,[2,†] R. Liotta,[2] R. Wyss,[2] and Y. M. Zhao [3,5,‡]

[1]*School of Arts and Sciences, Shanghai Maritime University, Shanghai 201306, China*

[2]*Department of Physics, Royal Institute of Technology (KTH), SE-10691 Stockholm, Sweden*

[3]*Department of Physics and Shanghai Key Laboratory of Particle Physics and Cosmology, Shanghai Jiao Tong University, Shanghai 200240, China*

[4]*Key Laboratory of Neutron Physics, Institute of Nuclear Physics and Chemistry, China Academy of Engineering Physics, Mianyang 621900, China*

[5]*Center of Theoretical Nuclear Physics, National Laboratory of Heavy Ion Accelerator, Lanzhou 730000, China*

(Received 13 November 2013; published 27 January 2014)

The magnetic moments of the first excited 2^+ state in even-even nuclei $^{102-130}$Sn and the low-lying yrast states in odd-mass nuclei $^{101-109,123-131}$Sn are calculated within the framework of the nucleon-pair approximation (NPA) of the shell model, by using the standard multipole-multipole interaction. Our calculations agree reasonably well with available experimental data. The $g(2_1^+)$ values, as well as the contributions from their spin and orbital angular momentum components, are evaluated in terms of the small NPA subspace spanned by S and D nucleon pairs. The magnetic moment is suggested to be a sensitive probe of the nuclear wave function in this region.

DOI: 10.1103/PhysRevC.89.014320 PACS number(s): 21.10.Re, 21.10.Ky, 21.60.Ev, 23.20.Lv

I. INTRODUCTION

Magnetic moments of low-lying states provide relevant information on the detailed single-particle configurations contributing to the nuclear wave function, particularly for semimagic nuclei around closed shells [1–9]. The tin isotopes provide us with one of the longest chains of semimagic nuclei currently accessible to nuclear structure studies [10–13]. In recent years, the magnetic moments of the first excited 2^+ state [denoted by $\mu(2_1^+)$, or alternatively its g factor denoted by $g(2_1^+)$] of tin isotopes with even neutron numbers have been of experimental interest [2–6]. Among these experiments, the $g(2_1^+)$ values of the stable isotopes $^{112-124}$Sn were studied by using transient field techniques [2–4]. Approaching towards the doubly magic ^{100}Sn and ^{132}Sn, the nuclei are radioactive and the corresponding experimental magnetic moments have been not available until the 2012–2013 experiments of ^{126,128}Sn in Refs. [5,6]. The general trend of measured $g(2_1^+)$ values in $^{112-126}$Sn runs from positive values for the lighter isotopes to negative values for the heavier ones. However, there are noticeable differences in magnitudes for a few $g(2_1^+)$ values obtained in different experiments.

A number of theoretical studies have been carried out to analyze $g(2_1^+)$ values in tin isotopes [3–6,14–18]. The quasiparticle random phase approximation (QRPA) calculations [15] on $^{114-132}$Sn predicted $g(2_1^+)$ values of $\sim -0.06\mu_N$ for $^{114-124}$Sn and $\sim +0.18\mu_N$ for ^{128}Sn. Relativistic quasiparticle random phase approximation (RQRPA) calculations [16] on $^{100-132}$Sn predicted a gradual decrease in $g(2_1^+)$ with the increase of mass number, i.e., positive values for $^{102-126}$Sn (from $\sim +0.4\mu_N$ at $A = 102$ to $\sim +0.03\mu_N$ at $A = 126$) and negative values for ^{128,130}Sn ($\sim -0.16\mu_N$ at $A = 130$). As pointed out in Refs. [3,6], the difference between the $g(2_1^+)$ predictions for these two models stems from the fact that the RQRPA calculation has a relatively large proton orbital contribution to the total wave function. Shell-model (SM) calculations have also been carried out for tin isotopes. Here we mention the studies of $^{116-124}$Sn in Ref. [3], $^{112-124}$Sn in Ref. [4], ^{124,126}Sn in Ref. [5], and $^{124-130}$Sn in Refs. [6,17]. The SM calculation of Ref. [4] on $^{112-124}$Sn, where ^{100}Sn was the inert core, described well the overall experimental trend of $g(2_1^+)$ values from positive for the lighter isotopes to negative for the heavier isotopes. The SM calculations of Refs. [5,6,17] predicted practically constant and negative $g(2_1^+)$ values ($\sim -0.12\mu_N$) for $^{124-130}$Sn.

The purpose of this paper is to apply the nucleon-pair approximation (NPA) [19] of the shell model to evaluate the magnetic moments of low-lying states for both even-even and odd-mass tin isotopes. The validity of this framework has been studied in many cases, e.g., single-j and many-j shells, semimagic and open-shell nuclei, phenomenological and effective interactions, etc., see Ref. [20] for a recent review. In recent years, the NPA has been successfully applied to study the low-lying states of even-even, odd-A, and odd-odd nuclei with $A \sim 80$ [21], 100 [22], 130 [23], and 210 [24]. In this model, the dimension of the collective nucleon-pair subspace is small, thus providing a simple and illuminating picture of the structure of the nuclei under investigation. As we will show below, the magnetic moment is very sensitive to the details of the wave function, as it happens quite often that only small components contribute to the corresponding matrix elements. Therefore magnetic moments provide a very powerful tool to test different models. In this work we will evaluate magnetic moments in the tin region and explore the role played by the leading NPA configurations.

The paper is organized as follows. In Sec. II a brief introduction to the NPA, including the form of Hamiltonian, its parameters, the construction of nucleon-pair subspace, and the evaluation of transition operators, is given. In Sec. III

*huijiang@shmtu.edu.cn

†chongq@kth.se

‡Corresponding author: ymzhao@sjtu.edu.cn

we present our calculations on the magnetic moments of the first excited 2^+ state in even-even nuclei $^{102-130}$Sn, and the low-lying yrast states in odd-mass nuclei $^{101-109,123-131}$Sn. A summary and conclusion are given in Sec. IV.

II. THEORETICAL FRAMEWORK

For medium-heavy nuclei the dimension of the shell model configuration space is prohibitively large, and one has to resort to various truncation schemes, e.g., the interacting boson model [25], the broken pair approximation [26], the fermion dynamical symmetry model [27], as well as the NPA [19]. In the NPA one diagonalizes the SM Hamiltonian in a truncated nucleon-pair subspace. If all possible nucleon pairs are considered, the results provided by the NPA coincide with those of the full shell model calculation [28].

In the NPA a collective pair with angular momentum r and projection M is defined as [19]

$$A^{(r)\dagger}_M = \sum_{jj'} y(jj'r)(C^\dagger_j \times C^\dagger_{j'})^{(r)}_M,$$

where $C^\dagger_j$ is the single-particle creation operator in the j orbit. $r = 0,2$ corresponds to S and D pairs, respectively. The numbers $y(jj'r)$ are the so-called structure coefficients of the nucleon pair with spin r.

The NPA Hamiltonian is chosen to have the form

$$H = \sum_j \epsilon_j C^\dagger_j C_j + G_0 \mathcal{P}^{(0)\dagger} \cdot \mathcal{P}^{(0)} + G_2 \mathcal{P}^{(2)\dagger} \cdot \mathcal{P}^{(2)} + \kappa Q \cdot Q,$$

where ϵ_j is the single-particle energy, G_0, G_2, and κ are the two-body interaction strengths corresponding to monopole, quadrupole pairing, and quadrupole-quadrupole interactions between valence neutrons. The pairing and quadrupole operators are defined as follows:

$$\mathcal{P}^{(0)\dagger} = \sum_j \frac{\sqrt{2j+1}}{2}(C^\dagger_j \times C^\dagger_j)^{(0)}_0,$$

$$\mathcal{P}^{(2)\dagger} = \sum_{jj'} q(jj')(C^\dagger_j \times C^\dagger_{j'})^{(2)}_M,$$

$$Q = \sum_{jj'} q(jj')(C^\dagger_j \times \tilde{C}_{j'})^{(2)}_M,$$

where $q(jj') = \frac{(-)^{j-1/2}}{\sqrt{20\pi}} \hat{j}\hat{j}' C^{20}_{j1/2,j'-1/2} \langle nl|r^2|nl'\rangle$ and $C^{20}_{j1/2,j'-1/2}$ is the Clebsch-Gordan coefficient.

The single-particle energies and two-body interaction parameters corresponding to the neutron excitations in our calculations are shown in Table I. The nuclei with mass number $A < 116$ are treated in terms of valence neutron particles, and those with $A \geq 116$ in terms of valence neutron holes, as in Ref. [22]. In Table I the neutron single-particle energies $g_{7/2}$ and $d_{5/2}$ are taken from the experimental excitation energies of ^{101}Sn [29]. There are no experimental data for the remaining orbitals, and we take those single-particle energies from a previous shell model calculation [30]. The neutron hole single-particle energies are also extracted from the corresponding experimental excitation energies of ^{131}Sn [31]. The two strengths G_0 of the monopole interactions in Table I are the same as in previous calculations in these nuclear regions [22]. The remaining four parameters corresponding to the quadrupole interactions, i.e., the values of G_2 and κ, are obtained by adjusting the experimental excited energies and electromagnetic properties of low-lying states. For the odd-mass nuclei, we assume the same parameters as their even-even core.

TABLE I. Single-particle (s.p.) energies ϵ_j (in MeV) and two-body interaction parameters G_0, G_2, κ. The unit of G_0 is MeV; the units of G_2 and κ are MeV/r_0^4, $r_0^2 = 1.012A^{1/3}$ fm^2. All two-body interaction parameters are negative, and we remove the minus sign here for short.

Nucleus	$\epsilon_{s_{1/2}}$	$\epsilon_{d_{3/2}}$	$\epsilon_{d_{5/2}}$	$\epsilon_{g_{7/2}}$	$\epsilon_{h_{11/2}}$	G_0	G_2	κ
$A < 116$	1.550	1.660	0.172	0.000	3.550	0.180	0.018	0.039
$A \geq 116$	0.332	0.000	1.655	2.434	0.065	0.131	0.010	0.012

The magnetic dipole moment is given by

$$\mu(\beta,J) = C^{JJ}_{JJ,10}\langle \beta,J||g_{l\nu}L_\nu + g_{s\nu}S_\nu||\beta,J\rangle,$$

where $|\beta,J\rangle$ is the eigenfunction carrying angular momentum J and the symbol β represents all quantum numbers other than J. $g_{l\nu}$ and $g_{s\nu}$ are, respectively, the effective orbital and spin gyromagnetic ratios. The value of $g_{s\nu}$ is taken to be $-3.826 \times 0.7\mu_N$, where the number 0.7 is the conventional quenching factor. The effective orbital gyromagnetic ratio is $g_{l\nu} = 0.09\mu_N$ for $A < 116$ and $0.015\mu_N$ for $A \geq 116$, which are optimized by a χ^2 fitting of experimental data. In the present calculation we choose the experimental g factors of ^{112,114}Sn in Ref. [4], ^{122}Sn in Ref. [2], and ^{124,126,128}Sn in Ref. [6]. It is relevant to point out that gyromagnetic ratios we use here for $A \geq 116$ are similar to the ones adopted in Ref. [32], where it is pointed out that these parameters take into account core polarization as well as meson-exchange current effects. The g factor is defined by μ/J.

The total orbital angular momentum operator L_ν and total spin S_ν can be identified with collective dipole operators as follows:

$$L_\nu = Q^1_{l\nu} = \sum_{jj'} q_l(jj'1)(C^\dagger_j \times \tilde{C}_{j'})^{(1)},$$

$$S_\nu = Q^1_{s\nu} = \sum_{jj'} q_s(jj'1)(C^\dagger_j \times \tilde{C}_{j'})^{(1)},$$

with

$$q_l(jj'1) = (-1)^{l+1/2+j'}\sqrt{\frac{l(l+1)}{3}}\hat{j}\hat{j}'\hat{l}\begin{Bmatrix} j & j' & 1 \\ l & l & 1/2 \end{Bmatrix},$$

$$q_s(jj'1) = (-1)^{l+1/2+j}\frac{1}{\sqrt{2}}\hat{j}\hat{j}'\begin{Bmatrix} j & j' & 1 \\ 1/2 & 1/2 & l \end{Bmatrix}.$$

Here $l = l'$ because the L_ν and S_ν operators cannot change the orbital angular momentum. Here we take the Rose convention for the reduced matrix element $\langle j||g_{l\nu}L_\nu + g_{s\nu}S_\nu||j'\rangle$. For our purpose it is important to mention that $\langle j||g_{l\nu}L_\nu + g_{s\nu}S_\nu||j'\rangle$ does not vanish only between the same

single-particle sates ($j = j'$) or spin-orbit partners ($j = l \mp 1/2 \rightarrow j' = l \pm 1/2$) [33]. Therefore within the model space to be considered in this paper, the cases $j = j'$ or $j = d_{5/2}$, $j' = d_{3/2}$ (or vice versa) provide nonvanishing values to the matrix element. This is the reason why the magnetic moment is an excellent probe of the wave function. We will come back to this in the next section.

Because we focus on the $g(2_1^+)$ values, our subspace is constructed by S and D nucleon pairs of neutron particles (or neutron holes) with respect to the doubly closed shell nucleus ^{100}Sn and ^{132}Sn. As in Ref. [24], we obtain the structure coefficients in even-even nuclei $^{102-114}$Sn and $^{118-130}$Sn based on a variational procedure as follows. For S pairs, we diagonalize the Hamiltonian H in the noncollective space $(S_j^\dagger)^N|0\rangle$, with j running over all single-particle levels. Our structure coefficients are determined by using the χ^2-fitting procedure, such that the state $(S^\dagger)^N|0\rangle$ has the maximum overlap with the ground state. For D pairs, we diagonalize the same H in the $(S^\dagger)^{N-1}D^\dagger_{j_1,j_2}|0\rangle$ space, corresponding to $(j_1 j_2)_{2^+}$, with j_1, j_2 running over all single-particle levels ($j_1 \leq j_2$), and S represents the collective S pair calculated above. The structure coefficients of collective D pairs are determined based on the energetically lowest eigenstate. Such a variational procedure would require a prohibitively long computing time in the case of ^{116}Sn. Therefore we use in this nucleus the very simple BCS approach to determine our S pairs. This is reasonable since these pairs are just pairing (monopole) excitations. The D pairs of ^{116}Sn are obtained by using the commutator $D^\dagger = \frac{1}{2}[Q, S^\dagger]$ [26]. The structure coefficients of odd-mass nuclei are taken to be the same as those of their even-even core.

III. CALCULATIONS AND DISCUSSIONS

In this section we present the calculated magnetic dipole moments, corresponding to the first 2^+ states of even-even nuclei $^{102-130}$Sn and a few low-lying states of odd-mass nuclei $^{101-109,123-131}$Sn.

Our calculated $g(2_1^+)$ values in even-even tin isotopes are shown in Fig. 1. Experimental data are those reported by Hass [2], East [3], Walker [4], Kumbartzki [5], and Allmond [6]. Our results are denoted by blue squares. Results of other theoretical works (QRPA [15], RQRPA [16], SM 2011 [4], and SM 2013 [6]) are also presented for comparison. It is seen that our calculated results agree well with the corresponding experimental values, except for ^{118}Sn and ^{128}Sn, but even here the disagreement is not very remarkable. One has to point out that the experimental errors are big and that in ^{112}Sn different experiments provide different $g(2_1^+)$ values. In this particular case our calculation agrees better with the value reported in Ref. [4], as seen in the figure.

The S and D pairs play a dominant role in the building up of the 2_1^+ states. In our case, we found that more than 90% of the contributions to the $g(2_1^+)$ values originate from the $|(S^\dagger)^{N-1}D^\dagger\rangle$ configuration. To understand the structure of these states, we analyze the partial contribution of the 2_1^+ configurations to the g factor as follows. We diagonalize the same H in the $(S^\dagger)^{N-1}D^\dagger_{j_1,j_2}|0\rangle$ subspace, with j_1, j_2 running over all

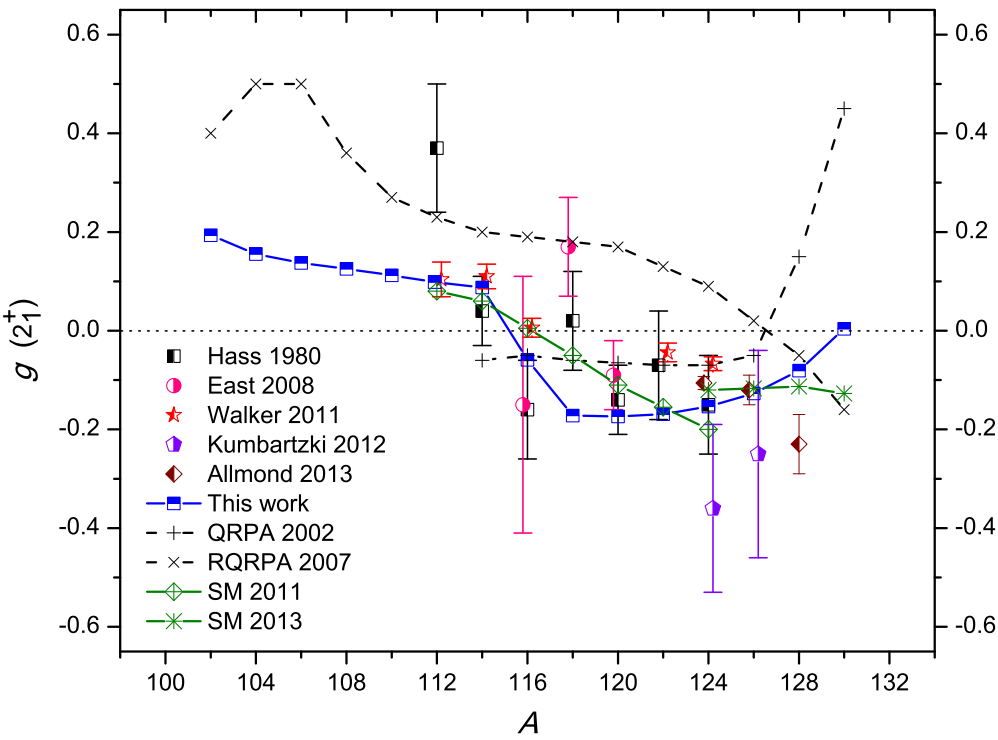

FIG. 1. (Color online) The $g(2_1^+)$ values (in unit of μ_N) of even-even tin isotopes. Experimental data include Hass 1980 [2], East 2008 [3], Walker 2011 [4], Kumbartzki 2012 [5], and Allmond 2013 [6]. Our results are shown as squares in blue. Results of other theoretical works (QRPA 2002, RQRPA 2007, SM 2011, and SM 2013) are taken from Refs. [15], [16], [4], and [6], respectively.

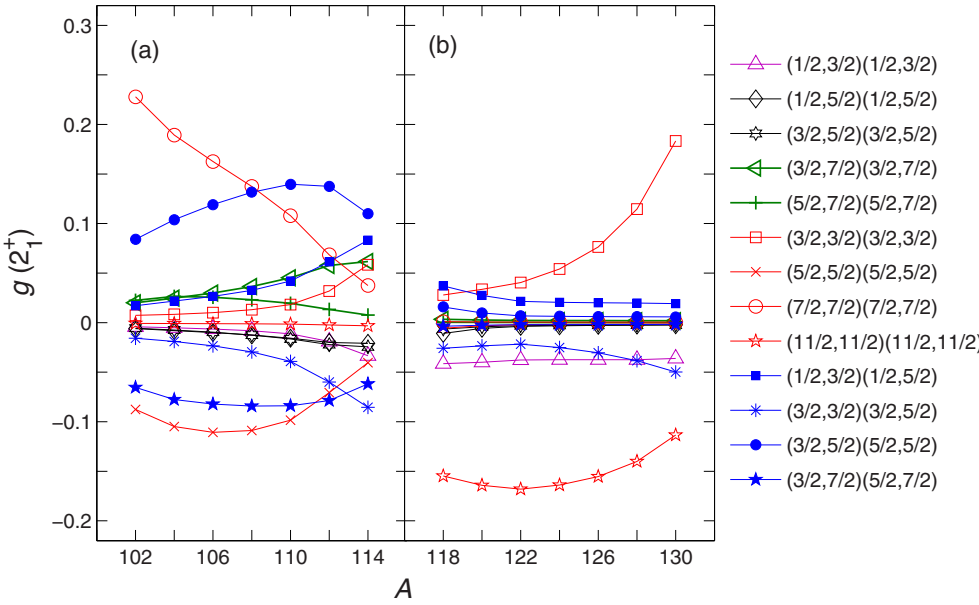

FIG. 2. (Color online) All possible nonvanishing components $g(j_1 j_2,2^+; j_3 j_4,2^+)$ [in Eq. (1)] corresponding to $g(2_1^+)$ values (in unit of μ_N) as a function of A in tin isotopes. The values of the nondiagonal amplitudes, i.e., with $[(j_1, j_2) \neq (j_3, j_4)]$, are given in blue. Notice that in this case the different states are always in the combination ($j_1 = d_{3/2}$, $j_3 = d_{5/2}$) or ($j_2 = d_{3/2}$, $j_4 = d_{5/2}$). The diagonal amplitudes, i.e., $[(j_1, j_2) = (j_3, j_4)]$, are also given.

single-particle orbits that couple to 2^+. The eigenfunction of the 2_1^+ state is given by $|2_1^+\rangle = \sum_{j_1 j_2} X_{j_1 j_2} |(S^\dagger)^{N-1} D^\dagger_{j_1,j_2}|0\rangle$. And the $g(2_1^+)$ value is expressed as

$$\begin{aligned} g(2_1^+) &= \frac{C^{22}_{22,10}}{2} \langle 2_1^+ || g_{l\nu} L_\nu + g_{s\nu} S_\nu || 2_1^+ \rangle \\ &= \sum_{j_1 j_2, j_3 j_4} \langle 0|(S^\dagger)^{N-1} D^\dagger_{j_1,j_2} || M || (S^\dagger)^{N-1} D^\dagger_{j_3,j_4}|0\rangle \\ &= \sum_{j_1 j_2, j_3 j_4} g(j_1 j_2,2^+; j_3 j_4,2^+), \end{aligned} \quad (1)$$

with

$$M = \frac{C^{22}_{22,10}}{2} \left[X_{j_1 j_2} (g_{l\nu} L_\nu + g_{s\nu} S_\nu) X_{j_3 j_4} \right].$$

According to the above discussion in relation to the matrix element $\langle j || g_{l\nu} L_\nu + g_{s\nu} S_\nu || j' \rangle$, the component $g(j_1 j_2,2^+; j_3 j_4,2^+)$ vanishes unless $j_1 = j_3$, $j_2 = j_4$ or $j_1 = d_{3/2}$, $j_3 = d_{5/2}$, $j_2 = j_4$, or $j_2 = d_{3/2}$, $j_4 = d_{5/2}$, $j_1 = j_3$. As a result, only the 13 contributions to $g(2_1^+)$ shown in Fig. 2(a) for $A < 116$ and (b) for $A > 116$ are nonvanishing.

One notices that the main contributions are provided in large part from the most relevant single-particle valence states: the shells $g_{7/2}$, $d_{5/2}$ for $A < 116$ and $d_{3/2}$, $h_{11/2}$ for $A > 116$. Thus in light isotopes of Fig. 2(a), up to $A = 108$, the largest contributions are from $(g_{7/2}g_{7/2})(g_{7/2}g_{7/2})$ and $(d_{5/2}d_{5/2})(d_{5/2}d_{5/2})$, as expected according to the location of the shells $g_{7/2}$ and $d_{5/2}$ in the spectrum of Table I. But it is not straightforward that the contribution from $(d_{5/2}g_{7/2})(d_{5/2}g_{7/2})$ (green line with crosses) would be very small. What is also unexpected is that the nondiagonal contributions (the blue lines in the figure), all of which involve the high-lying shell $d_{3/2}$ and even the shell $s_{1/2}$, should have such important influence. As the number of neutrons increases, high-lying shells become important. Thus for $A \geq 110$ the contributions of the shells $d_{3/2}$ and $s_{1/2}$ are gradually increasing. But also here it is to be noted the unexpected large contribution corresponding to $(d_{3/2}d_{5/2})(d_{5/2}d_{5/2})$.

For $A > 116$ one expects that, according to the single-particle energies of Table I, the most important shells would be $d_{3/2}$, $h_{11/2}$, and $s_{1/2}$ (in that order). And indeed one sees in Fig. 2(b) that the largest contributions are from $(d_{3/2}d_{3/2})(d_{3/2}d_{3/2})$ and $(h_{11/2}h_{11/2})(h_{11/2}h_{11/2})$.

To analyze farther the structure of $g(2_1^+)$ values we present in Fig. 3 the partial sum of all diagonal and nondiagonal contributions. One sees in this figure that the global trend of $g(2_1^+)$ values is determined by the diagonal elements. Another important feature here is that close to $A = 114$ and $A = 130$ both contributions are about the same and small. However, the corresponding partial contributions, seen in Fig. 2, are large but out of phase. In the particular case that we analyze here, the states 2_1^+ in tin isotopes are classical examples of "collective" (or vibrational) excitations from the viewpoint of $E2$ electromagnetic transition probes. That is, in the evaluation of the $B(E2; 0_1^+ \rightarrow 2_1^+)$ [denoted by $B(E2\uparrow)$] transition matrix elements all wave function components contribute with the same phase and, therefore, the precision to which those components are evaluated are not crucial. In the corresponding calculation of $g(2_1^+)$ values the components contribute out of phase and one may thus get large errors if those components are not precisely evaluated.

So far we have discussed the general trend of g factors. We will now analyze in more detail the most important features resulting from a comparison between the experimental and theoretical results. One of these outstanding features is the

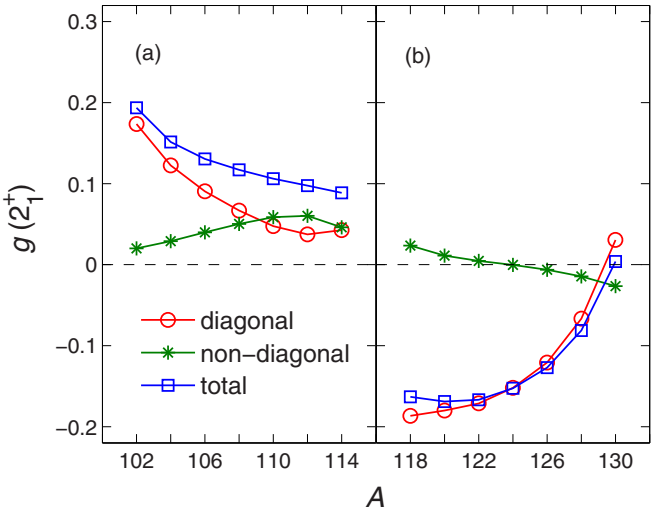

FIG. 3. (Color online) Diagonal and nondiagonal elements contributions to total $g(2_1^+)$ values (in units of μ_N) of even-even tin isotopes in (a) $A < 116$ and (b) $A > 116$.

measured magnetic moment in the nucleus ^{112}Sn, which is the lightest tin isotope for which such measurement has so far been performed. According to Ref. [2] it is $g(2_1^+) = +0.37(13)\mu_N$. But a more recent measurement [4] provided a very different result for this quantity, i.e., $g(2_1^+) = +0.104(35)\mu_N$ [4]. In this reference it was suggested that the configurations $g_{7/2}^2$ and $d_{5/2}g_{7/2}$ should contribute significantly to the building up of the state 2_1^+ because the empirical g factor corresponding to these configurations is $g_{\rm emp} \approx +0.2\mu_N$, which is consistent with the experimental positive value. However our calculation, which fits very well the experimental value given in this reference, shows [Fig. 2(a) at $A = 112$] that all partial contributions cancel out, except $(d_{3/2},d_{5/2})(d_{5/2},d_{5/2})$, for which the g factor is $g(2_1^+) \sim +0.13\mu_N$. That is, neither $g_{7/2}^2$ nor $d_{5/2}g_{7/2}$ contribute by themselves to the g factor. It is seen that the configuration $g_{7/2}^2$ carries the small and positive g factor of $\sim+0.06\mu_N$. The contribution of the configuration $d_{5/2}g_{7/2}$ is included in the diagonal element $(5/2,7/2)(5/2,7/2)$ and in the nondiagonal one $(3/2,7/2)(5/2,7/2)$. Their g factors are nearly zero and $\sim-0.07\mu_N$, as seen in the figure.

In our calculations, the g factor of ^{114}Sn is similar to that of ^{112}Sn. One sees in Fig. 2(a) that in this case many configurations contribute with similar magnitude, but different signs, resulting in the final value of $g(2_1^+) \sim +0.09\mu_N$ (see also Fig. 3).

Crossing the nucleus ^{116}Sn, the observed $g(2_1^+)$ value decreases from a positive to a negative value, as seen in Fig. 1. It is suggested that the $d_{3/2}s_{1/2}$ configuration, with its empirical g factor of $\sim-0.11\mu_N$, should be important in the state ^{116}Sn(2_1^+). This may explain the negative value of the g factor [3,4]. However, Fig. 2(b) shows that for nuclei from ^{118}Sn to ^{122}Sn the reason of the negative value of the magnetic moment is due to the dominance of the shell $h_{11/2}$.

In the heavier nuclei, up to ^{130}Sn, it is the interplay between the shells $h_{11/2}$ and $d_{3/2}$ which determines the g factor. But there is a very important exception to this trend, and it is the positive and rather large measured g factor in ^{118}Sn [2,3]. One sees in Fig. 1 that the predictions of the QRPA [15], the SM [4], and this work are all negative in this case. However the RQRPA calculations [16] agree well with the experiment because of a

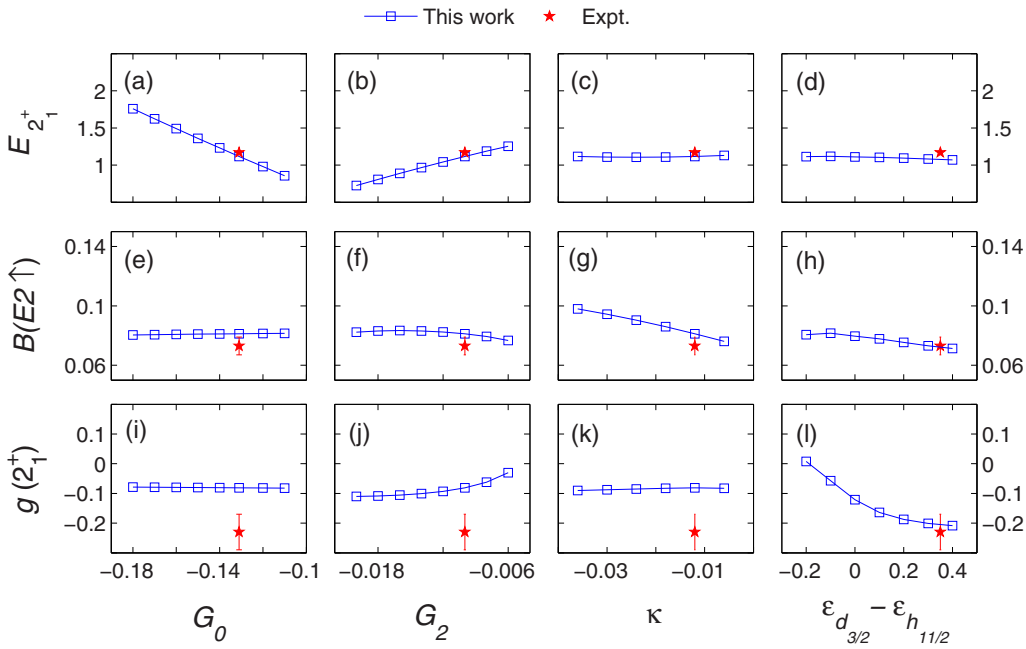

FIG. 4. (Color online) Excitation energy $E_{2_1^+}$ (in MeV), $B(E2;0_1^+ \to 2_1^+)$ [denoted by $B(E2\uparrow)$] value (in e^2b^2) and $g(2_1^+)$ value (in μ_N) in the nucleus ^{128}Sn as a function of the two-body interaction strengths G_0, G_2, and κ as well as the relative single-particle energy $\epsilon_{d_{3/2}} - \epsilon_{h_{11/2}}$ (in MeV). In each case all parameters, except the variable considered, are as in Table I. Experimental data are taken from: $E_{2_1^+}$ [31], $B(E2\uparrow)$ [34], and $g(2_1^+)$ [6]. The value of the effective charge is $-0.95e$ [22].

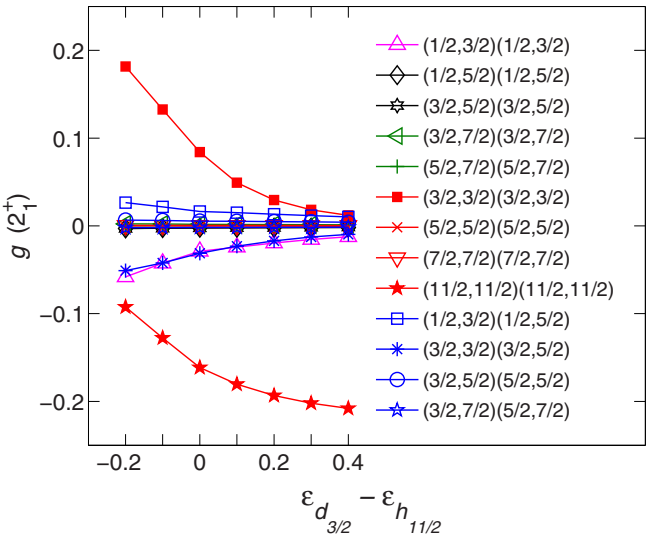

FIG. 5. (Color online) Same as Fig. 2 but for the nucleus ^{128}Sn as a function of $\epsilon_{d_{3/2}} - \epsilon_{h_{11/2}}$ (in MeV).

relatively large proton contribution to the total wave function. From Fig. 2(b) one sees that for heavier isotopes the shell $d_{3/2}$, with a positive g factor, becomes relevant. This is also pointed out in Refs. [3,4]. We have performed calculations by varying the two-body interactions to improve our result in this nucleus. But the calculated negative g factor is found to be very robust. Therefore further investigation for this state is necessary both experimentally and theoretically.

In ^{128}Sn our g factor is outside the experimental error. We tried to improve this situation, while keeping all other experimental quantities in agreement with the corresponding data, by varying the parameters that define the dynamics of our calculations within reasonable limits. For this we calculated in the nucleus ^{128}Sn the corresponding $g(2_1^+)$ value as well as the excitation energy $E_{2_1^+}$ and the $B(E2\uparrow)$ value as a function of the strength of the interactions, i.e., G_0, G_2, and κ, and also of the energy difference $\epsilon_{d_{3/2}} - \epsilon_{h_{11/2}}$. The rest of the parameters in Table I were kept unchanged. The results are shown in Fig. 4, with experimental data taken from $E_{2_1^+}$ [31], $B(E2\uparrow)$ [34], and $g(2_1^+)$ [6]. One sees in this figure that the calculated and experimental values of the energy $E_{2_1^+}$ and of the $B(E2\uparrow)$ strength coincide just for the interaction parameters given in Table I. However, there is not any value of these parameters that provides a reasonable g factor. Only when the relative position of the shells $\epsilon_{d_{3/2}}$ and $\epsilon_{h_{11/2}}$ (which in Table I is $\epsilon_{d_{3/2}} - \epsilon_{h_{11/2}} = -0.065$ MeV) is changed by about 0.4 MeV does one get the experimental g factor, which is $g(2_1^+) = (-)0.23(6)\mu_N$ (with its sign not well established) [6]. It is also remarkable that the values of $E_{2_1^+}$ and $B(E2\uparrow)$ are practically independent of the difference $\epsilon_{d_{3/2}} - \epsilon_{h_{11/2}}$. It has to be mentioned that large-scale shell-model calculations [6,17] reported the value $g(2_1^+) \sim -0.11\mu_N$ by using $\epsilon_{d_{3/2}} - \epsilon_{h_{11/2}} = -0.07$ MeV (see Fig. 1).

In Fig. 5, we present the partial contribution to the g factor of all possible configurations as a function of $\epsilon_{d_{3/2}} - \epsilon_{h_{11/2}}$ in ^{128}Sn. The remarkable feature in this figure is that as $\epsilon_{d_{3/2}} - \epsilon_{h_{11/2}}$ approaches the value of 0.4 MeV, for which the theoretical g factor fits the corresponding experimental value, the contribution of the shell $d_{3/2}$ becomes negligible. As a result of this the shell $h_{11/2}$ becomes overwhelmingly dominant and the g factor becomes relatively large and negative, as required in Fig. 1. This suggests that the single-particle state $\epsilon_{d_{3/2}}$ should lie higher than the state $\epsilon_{h_{11/2}}$ in this case.

To analyze this further we present in Fig. 6 the calculated $E_{2_1^+}$, $B(E2\uparrow)$, and $g(2_1^+)$ values as a function of the energy difference $\epsilon_{d_{3/2}} - \epsilon_{h_{11/2}}$ for ^{130,128,126,124}Sn. It is seen that the values of $E_{2_1^+}$ and $B(E2\uparrow)$ are also independent of the difference $\epsilon_{d_{3/2}} - \epsilon_{h_{11/2}}$ for ^{130,126,124}Sn, the same as that for ^{128}Sn. However the g factor is less sensitive to $\epsilon_{d_{3/2}} - \epsilon_{h_{11/2}}$ as valence neutron-holes increase, with the quickest change occurring in ^{130}Sn. Therefore, if the single-particle state $\epsilon_{d_{3/2}}$ lies higher than the state $\epsilon_{h_{11/2}}$, our g factors of $^{128-124}$Sn will agree well with the experiment, but the calculated result of ^{130}Sn will now be negative ($\sim -0.2\mu_N$). Future measurements with improved precision in ^{128}Sn, as well as the experimental $g(2_1^+)$ data in ^{130}Sn, are highly desirable to clarify the physics of the 2_1^+ states in even-even tin isotopes.

In Fig. 7, we present the spin and orbital angular momentum contributions to the total g factor. One sees in this figure that the overall trend of g factors as a function of A is mainly determined by the spin contribution. This is also pointed out in the RQRPA calculation [16]. The orbital contribution is practically constant for the case $A < 116$ and negligible for $A > 116$. It is important to stress that the constant value of the orbital contribution in light tin isotopes is very important to obtain good agreement between theory and experiment in these nuclei, as seen in Fig. 1. It is also interesting to notice that the spin contribution approaching $A = 114$ vanishes and therefore the g factors of ^{112}Sn and ^{114}Sn are practically due to the corresponding orbital part. For heavy tin isotopes the situation is the opposite. Here it is the spin contribution that determines the g factor.

In Table II we present the calculated magnetic moments μ corresponding to yrast states in odd-mass tin isotopes. These are $5/2_1^+$, $7/2_1^+$ in $^{101-109}$Sn, and $3/2_1^+$, $11/2_1^-$ in $^{123-131}$Sn. Experimental data [36] and shell-model calculations [37] are also listed for comparison. One sees in this table that our results agree well with the existing experimental data as well as with the SM calculated results.

The $11/2_1^-$ state is simple and its μ value remains constant as a function of A. For the states $5/2_1^+$, $7/2_1^+$, and $3/2_1^+$ the μ values decrease slightly with increasing valence neutron number. This indicates that the wave functions of these states change slowly as A increases, as expected in this typical BCS region. This can also be readily understood within the NPA, since the dominant NPA configurations corresponding to the $5/2_1^+$, $7/2_1^+$ states in $^{101-109}$Sn, and to the states $3/2_1^+$, $11/2_1^-$ in $^{123-131}$Sn are $|(d_{5/2})S^N\rangle$, $|(g_{7/2})S^N\rangle$, $|(d_{3/2})S^N\rangle$, and $|(h_{11/2})S^N\rangle$, respectively. Therefore these states are determined by the unpaired neutron, which provides a nearly constant value of μ.

One also sees in Table II that the experimental values of $\mu(3/2_1^+)$ and $\mu(11/2_1^-)$ in nuclei $^{123-131}$Sn increase slightly with valence neutron hole number, in contrast to the predictions

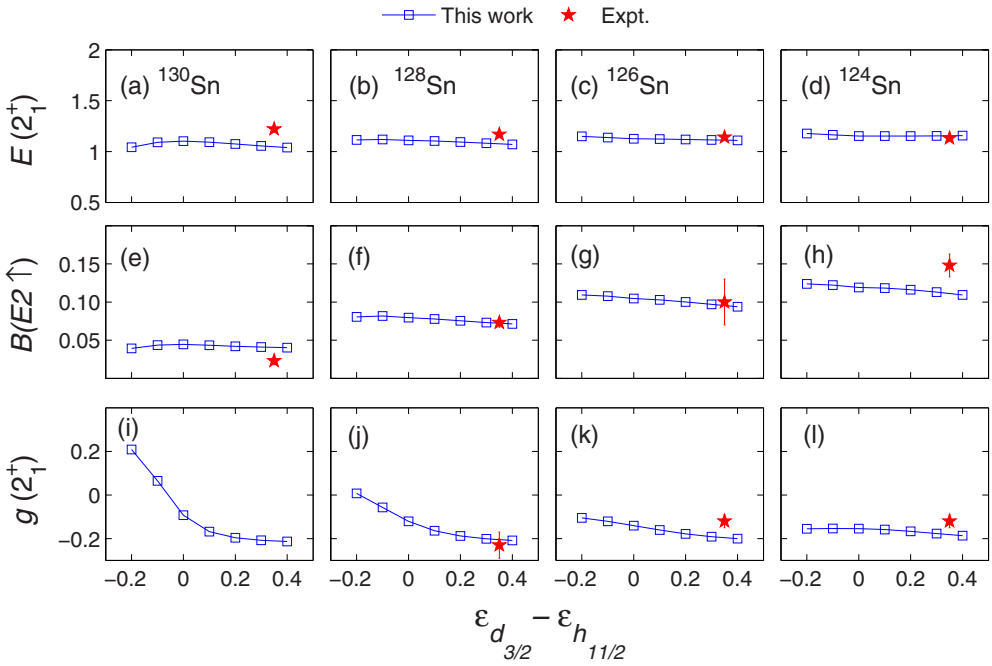

FIG. 6. (Color online) Same as Fig. 4 but for the nuclei ^{130,128,126,124}Sn as a function of $\epsilon_{d_{3/2}} - \epsilon_{h_{11/2}}$ (in MeV). Experimental data are taken from: $E_{2_1^+}$ [31], $B(E2\uparrow)$ [34,35], and $g(2_1^+)$ [6].

of the NPA and the SM. However, this difference is small compared to the overall good agreement between the theoretical results and experiments as already pointed out in Ref. [6]. It is interesting to point out that our calculated $\mu(3/2_1^+)$ values increase slightly with the energy difference $\epsilon_{d_{3/2}} - \epsilon_{h_{11/2}}$.

The spin of the ground and first excited states in ^{103}Sn [31] are $5/2_1^+$ and $7/2_1^+$, respectively. These spins are reversed with respect to those in ^{101}Sn [29]. It was suggested in Ref. [37] that the $J = 6$ two-body matrix elements $\langle 0g_{7/2}^2|V|0g_{7/2}^2\rangle_{J=6}$ and $\langle 0g_{7/2}1d_{5/2}|V|0g_{7/2}1d_{5/2}\rangle_{J=6}$ contribute to most of the spin inversion in ^{103}Sn. We analyzed within the NPA the impact of these two matrix elements upon the spin inversion and the μ values. We found that they indeed play a dominant role in the spin inversion in ^{103}Sn, but have little effect on $\mu(5/2_1^+)$ and $\mu(7/2_1^+)$.

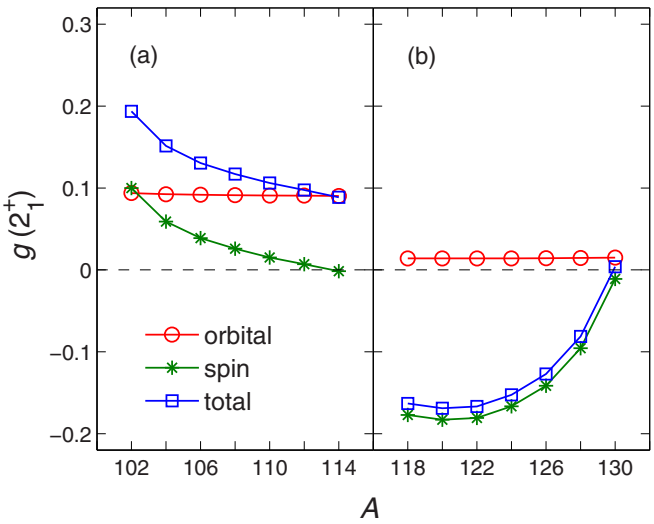

FIG. 7. (Color online) Spin and orbital contributions to total $g(2_1^+)$ values (in units of μ_N) of even-even tin isotopes in (a) $A < 116$ and (b) $A > 116$.

TABLE II. The magnetic moments μ (in unit of μ_N) in odd-mass tin isotopes. Experimental data and shell-model results are taken from Refs. [36] and [37], respectively.

	J^π	NPA	SM	Expt.
^{101}Sn	$5/2_1^+$	−1.158	–	
	$7/2_1^+$	+1.393	–	
^{103}Sn	$5/2_1^+$	−1.151	−1.299	
	$7/2_1^+$	+1.392	+1.014	
^{105}Sn	$5/2_1^+$	−1.141	−1.206	
	$7/2_1^+$	+1.388	+0.993	
^{107}Sn	$5/2_1^+$	−1.118	−1.114	
	$7/2_1^+$	+1.379	+0.942	
^{109}Sn	$5/2_1^+$	−1.084	−1.024	−1.079(6)
	$7/2_1^+$	+1.365	+0.924	
^{123}Sn	$3/2_1^+$	+0.796	+0.703	
	$11/2_1^-$	−1.264	−1.298	−1.3700(9)
^{125}Sn	$3/2_1^+$	+0.801	+0.750	+0.764(3)
	$11/2_1^-$	−1.264	−1.306	−1.348(6)
^{127}Sn	$3/2_1^+$	+0.808	+0.774	+0.757(4)
	$11/2_1^-$	−1.264	−1.319	−1.329(7)
^{129}Sn	$3/2_1^+$	+0.817	+0.789	+0.754(6)
	$11/2_1^-$	−1.264	−1.335	−1.297(5)
^{131}Sn	$3/2_1^+$	+0.831	+0.804	+0.747(4)
	$11/2_1^-$	−1.264	−1.339	−1.276(5)

Besides the states in Table II, the $1/2_1^+$ states in $^{101-109}$Sn and $^{123-131}$Sn are also found to be very simple within the NPA. Their dominant configuration in all those isotopes is $|(s_{1/2})S^N\rangle$. Our calculated μ values of this state are -1.339, -1.125,-1.332, -1.073, $-0.891\mu_N$ for $^{101-109}$Sn and -1.245, -1.268, -1.292, -1.316, $-1.339\mu_N$ for $^{123-131}$Sn, respectively.

IV. SUMMARY

In this paper we have calculated the magnetic moments of low-lying states for both even-even and odd-mass tin isotopes by using the SD-pair approximation (NPA) of the nuclear shell model. For the Hamiltonian we employed a monopole and quadrupole pairing plus quadrupole-quadrupole interaction with optimized parameters. On the one hand, the NPA approach generally well reproduces experimental data, and on the other hand, due to the very small subspace spanned by the NPA basis, the calculations can be performed in a rather straightforward fashion, thus allowing one to easily understand the physics behind the results.

We considered the region $A < 116$ independently of the one for $A \geq 116$, as seen in Table I. In the first case the lowest lying $g_{7/2}$ and $d_{5/2}$ shells are nearly degenerate. In the same fashion the lowest lying $h_{11/2}$ and $d_{3/2}$ shells are nearly degenerate in the second case. Not surprisingly, we found that near $A = 100$ the $g(2_1^+)$ values are practically determined by the $g_{7/2}$ and $d_{5/2}$ shells, but already starting at $A = 108$ the rather high-lying $d_{3/2}$ shell becomes important. Instead, in the $A > 116$ case the $h_{11/2}$ shell is important all through, but already at $A = 122$ the $d_{3/2}$ shell starts to have relevance. In both regions there is a strong cancelation among the contributions of different shells, which makes the magnetic moment a powerful tool to probe the corresponding wave function.

Experimentally one sees a strong transition in the g factors of the 2_1^+ state when crossing the nucleus ^{116}Sn. For $A < 116$ the g factors are positive while for $A \geq 116$ they are negative. This is a result of the influence of the $h_{11/2}$ shell, which carries a negative magnetic moment. Interestingly, we found that this shell has a too strong preponderance in our calculation, especially at the end of the shell, approaching the isotope ^{128}Sn, where the experimental g factor is too negative. We concluded that this feature indicates that the $h_{11/2}$ shell is located too high in the set of single-particle states in Table I. We arrived at this conclusion by evaluating the energies $E_{2_1^+}$ and the values of $B(E2\uparrow)$, besides the $g(2_1^+)$ values, as a function of different Hamiltonian parameters for ^{130,128,126,124}Sn.

We investigated also the spin and orbital angular momentum contributions to the $g(2_1^+)$ value and found that its overall trend with A is mostly determined by the spin contribution. The orbital part is practically constant in the region $A < 116$, but its value is fundamental to explain the experimental g factor. In the region $A > 116$ the orbital contribution is negligible and all g factors are given by the spin contribution. But also here when approaching the closed shell, at $A = 130$, the spin contribution disappears and as a results the g factor is nearly zero. As mentioned above, we found that this distinct feature is due to a too strong influence of the $h_{11/2}$ shell.

Our calculated magnetic moments μ corresponding to the $5/2_1^+$ and $7/2_1^+$ states in $^{101-109}$Sn as well as the $3/2_1^+$ and $11/2_1^-$ states in $^{123-131}$Sn are found to be determined by the unpaired nucleon in these odd neutron isotopes.

ACKNOWLEDGMENTS

This work was supported by the National Natural Science Foundation of China (Grant Nos. 11145005, 11225524, 11247241, 11305101, and 11305151), and the 973 Program of China (Grant No. 2013CB834401). C.Q., R.L., and R.W. acknowledge the support of the Swedish Research Council (VR) under Grants No. 621-2010-4723, 621-2012-3805, and 621-2013-4323. H.J. thanks the Shanghai Key Laboratory of Particle Physics and Cosmology (Grant No. 11DZ2260700) and KTH for financial support. Discussions with B. Cederwall and T. Bäck are gratefully acknowledged.

[1] N. Benczer-Koller and G. J. Kumbartzki, J. Phys. G: Nucl. Part. Phys. **34**, R321 (2007), and references therein.
[2] M. Hass, C. Broude, Y. Niv, and A. Zemel, Phys. Rev. C **22**, 97 (1980).
[3] M. C. East, A. E. Stuchbery, A. N. Wilson, P. M. Davidson, T. Kibédi, and A. I. Levon, Phys. Lett. B **665**, 147 (2008).
[4] J. Walker *et al.*, Phys. Rev. C **84**, 014319 (2011).
[5] G. J. Kumbartzki, N. Benczer-Koller, D. A. Torres, B. Manning, P. D. O'Malley, Y. Y. Sharon, L. Zamick, C. J. Gross, D. C. Radford, S. J. Q. Robinson, J. M. Allmond, A. E. Stuchbery, K.-H. Speidel, N. J. Stone, and C. R. Bingham, Phys. Rev. C **86**, 034319 (2012).
[6] J. M. Allmond, A. E. Stuchbery, D. C. Radford, A. Galindo-Uribarri, N. J. Stone, C. Baktash, J. C. Batchelder, C. R. Bingham, M. Danchev, C. J. Gross, P. A. Hausladen, K. Lagergren, Y. Larochelle, E. Padilla-Rodal, and C.-H. Yu, Phys. Rev. C **87**, 054325 (2013).
[7] K.-H. Speidel, S. Schielke, O. Kenn, J. Leske, D. Hohn, H. Hodde, J. Gerber, P. Maier-Komor, O. Zell, Y. Y. Sharon, and L. Zamick, Phys. Rev. C **68**, 061302(R) (2003).
[8] S. Schielke, D. Hohn, K.-H. Speidel, O. Kenn, J. Leske, N. Gemein, M. Offer, J. Gerber, P. Maier-Komor, O. Zell, Y. Y. Sharon, and L. Zamick, Phys. Lett. B **571**, 29 (2003).
[9] M. J. Taylor, N. Benczer-Koller, G. Kumbartzki, T. J. Mertzimekis, S. J. Q. Robinson, Y. Y. Sharon, L. Zamick, A. E. Stuchbery, C. Hutter, C. W. Beausang, J. J. Ressler, and M. A. Caprio, Phys. Lett. B **559**, 187 (2003).
[10] T. Faestermann, M. Górska, and H. Grawe, Prog. Part. Nucl. Phys. **69**, 85 (2013), and references therein.
[11] G. Guastalla *et al.*, Phys. Rev. Lett. **110**, 172501 (2013).
[12] V. M. Bader, A. Gade, D. Weisshaar, B. A. Brown, T. Baugher, D. Bazin, J. S. Berryman, A. Ekström, M. Hjorth-Jensen, S. R. Stroberg, W. B. Walters, K. Wimmer, and R. Winkler, Phys. Rev. C **88**, 051301(R) (2013).

[13] T. Bäck, C. Qi, B. Cederwall, R. Liotta, F. Ghazi Moradi, A. Johnson, R. Wyss, and R. Wadsworth, Phys. Rev. C **87**, 031306(R) (2013).
[14] R. J. Lombard, Nucl. Phys. A **114**, 449 (1968).
[15] J. Terasaki, J. Engel, W. Nazarewicz, and M. Stoitsov, Phys. Rev. C **66**, 054313 (2002).
[16] A. Ansari and P. Ring, Phys. Lett. B **649**, 128 (2007).
[17] B. A. Brown, N. J. Stone, J. R. Stone, I. S. Towner, and M. Hjorth-Jensen, Phys. Rev. C **71**, 044317 (2005).
[18] L. Y. Jia, H. Zhang, and Y. M. Zhao, Phys. Rev. C **75**, 034307 (2007); **76**, 054305 (2007).
[19] J. Q. Chen, Nucl. Phys. A **626**, 686 (1997); J. Q. Chen and Y. A. Luo, *ibid.* **639**, 615 (1998); Y. M. Zhao, N. Yoshinaga, S. Yamaji, J. Q. Chen, and A. Arima, Phys. Rev. C **62**, 014304 (2000).
[20] Y. M. Zhao and A. Arima, preprint (to be published).
[21] H. Jiang, G. J. Fu, Y. M. Zhao, and A. Arima, Phys. Rev. C **84**, 034302 (2011); G. J. Fu, J. J. Shen, Y. M. Zhao, and A. Arima, *ibid.* **87**, 044312 (2013).
[22] H. Jiang, Y. Lei, G. J. Fu, Y. M. Zhao, and A. Arima, Phys. Rev. C **86**, 054304 (2012); H. Jiang, C. Qi, Y. Lei, R. Liotta, R. Wyss, and Y. M. Zhao, *ibid.* **88**, 044332 (2013).
[23] Y. A. Luo and J. Q. Chen, Phys. Rev. C **58**, 589 (1998); N. Yoshinaga and K. Higashiyama, *ibid.* **69**, 054309 (2004).
[24] Z. Y. Xu, Y. Lei, Y. M. Zhao, S. W. Xu, Y. X. Xie, and A. Arima, Phys. Rev. C **79**, 054315 (2009); H. Jiang, J. J. Shen, Y. M. Zhao, and A. Arima, J. Phys. G: Nucl. Part. Phys. **38**, 045103 (2011).
[25] F. Iachello and A. Arima, *The Interacting Boson Model* (Cambridge University Press, Cambridge, 1987); F. Iachello and I. Talmi, Rev. Mod. Phys. **59**, 339 (1987).
[26] K. Allart, E. Boeker, G. Bonsignori, M. Saroia, and Y. K. Gambhir, Phys. Rep. **169**, 209 (1988).
[27] J. N. Ginocchio, Ann. Phys. (NY) **126**, 234 (1980); C.-L. Wu, Da Hsuan Feng, X.-G. Chen, J.-Q. Chen, and M. W. Guidry, Phys. Rev. C **36**, 1157 (1987).
[28] Y. Lei, Z. Y. Xu, Y. M. Zhao, and A. Arima, Phys. Rev. C **80**, 064316 (2009); **82**, 034303 (2010); Y. Lei, Y. M. Zhao, and A. Arima, *ibid.* **84**, 044301 (2011), and references therein.
[29] I. G. Darby, R. K. Grzywacz, J. C. Batchelder, C. R. Bingham, L. Cartegni, C. J. Gross, M. Hjorth-Jensen, D. T. Joss, S. N. Liddick, W. Nazarewicz, S. Padgett, R. D. Page, T. Papenbrock, M. M. Rajabali, J. Rotureau, and K. P. Rykaczewski, Phys. Rev. Lett. **105**, 162502 (2010).
[30] A. Banu *et al.*, Phys. Rev. C **72**, 061305(R) (2005).
[31] http://www.nndc.bnl.gov/ensdf/
[32] F. Le Blanc *et al.*, Phys. Rev. C **72**, 034305 (2005).
[33] R. D. Lawson, *Theory of the Nuclear Shell Model* (Clarendon Press, Oxford, 1980).
[34] D. C. Radford *et al.*, Nucl. Phys. A **746**, 83 (2004).
[35] A. Jungclaus *et al.*, Phys. Lett. B **695**, 110 (2011).
[36] N. J. Stone, At. Data Nucl. Data Tables **90**, 75 (2005).
[37] C. Qi and Z. X. Xu, Phys. Rev. C **86**, 044323 (2012).